IEEE Access
Multidisciplinary | Rapid Review | Open Access Journal

Date of publication xxxx 00, 0000, date of current version xxxx 00, 0000.

Digital Object Identifier 10.1109/ACCESS.2017.Doi Number

Cable Decoupling and Cable-Based Stiffening of Continuum Robots

Parsa Molaei[1], Graduate Student Member, IEEE, Nekita Pitts[1], Genevieve Palardy[1], Ji Su[2], Matthew K. Mahlin[3], James H. Neilan[4], and Hunter B. Gilbert[1], Member, IEEE

[1]Department of Mechanical and Industrial Engineering, Louisiana State University, Baton Rouge, LA 70803 USA
[2]Advanced Materials and Processing Branch, Research Directorate, NASA Langley Research Center, Hampton, VA 23681 USA
[3]Structural Mechanics and Concepts Branch, Research Directorate, NASA Langley Research Center, Hampton, VA 23681 USA
[4]Space Technology and Exploration Directorate, NASA Langley Research Center, Hampton, VA 23681 USA

Corresponding author: Hunter B. Gilbert (e-mail: hbgilbert@lsu.edu).

This work was supported by the Louisiana Space Grant Consortium under NASA Grant Number 80NSSC20M0110 and by the Louisiana Board of Regents under contract LEQSF(2020-24)-LaSPACE

ABSTRACT Cable-driven continuum robots, which are robots with a continuously flexible backbone and no identifiable joints that are actuated by cables, have shown great potential for many applications in unstructured, uncertain environments. However, the standard design for a cable-driven continuum robot segment, which bends a continuous backbone along a circular arc, has many compliant modes of deformation which are uncontrolled, and which may result in buckling or other undesirable behaviors if not ameliorated. In this paper, we detail an approach for using additional cables to selectively stiffen planar cable-driven robots without substantial coupling to the actuating cables. A mechanics-based model based on the planar Cosserat equations is used to find the design conditions under which additional cables can be routed without coupling of the cable lengths for small deformations. Simulations show that even for relatively large deformations, coupling remains small. A prototype is evaluated, and it is demonstrated that the compliance of the robot is substantially modified relative to the same robot without stiffening cables. Additional stiffening cables are shown to increase the end-effector output stiffness by a factor of approximately 10 over a typical design with actuating cables.

INDEX TERMS Tendon/wire mechanism, flexible robots, continuum robots, com-pliant joint mechanism

I. INTRODUCTION

Human space exploration is an essential mission of the National Aeronautics and Space Administration (NASA). The development of large and sustainable structures in space and for planetary habitats has been identified as one of the key enabling technologies as the next strategic thrust in space technology advancement. Various in-space assembly technologies have been being developed for making large space assets at NASA Langley Research Center. A cable-driven compliant space robotic technology has demonstrated unique capabilities and advantages in terms of flexibility, durability, and remote adjustability. The performance of the system can be optimized by the design of configuration and the selection of cable materials through modeling and experimental validation.

A. IN-SPACE ASSEMBLY

Advancing human space exploration entails developing larger and more sustainable structures in space and on other worlds requiring in-space manufacturing, assembly, and servicing. Identified as the next strategic thrust for the National Aeronautics and Space Administration (NASA), In-space Assembly Servicing and Manufacturing (ISAM) offers key possibilities by freeing a mission from the restrictions of mass and volume of current launch vehicles. It is also crucial to consider how to optimize assembly methods and agents being used to diversify what capabilities they must allow for a broad range of applications, minimizing launch cost.

NASA Langley Research Center's (LaRC) in-space assembly and autonomy researchers have been developing various technology capabilities required to make larger space assets. For example, in 2002, LaRC's Automated Telescope Assembly Lab (ASAL) autonomously assembled and

disassembled an 8-meter truss structure [1]. Recently research in in-space assembly has been ramping up with NASA funding technology development for three tipping point In-Space Robotic Manufacturing and Assembly (IRMA) projects, Dragonfly [2], Archinaut [3], and the Commercial Infrastructure for Robotic Assembly and Servicing (CIRAS) [4]. In Addition, the NASA in-Space Assembled Telescope (iSAT) Study recommended to the 2020 Astronomy and Astrophysics Decadal Survey that ISA be considered as a possible enabling method for future large space telescopes for its risk, cost, and science benefits [5].

In this effort, cable-driven systems have been developed, highlighted by the "Tendon-Acutated Lightweight In-Space MANipulator" (TALISMAN) developed by LaRC. TALISMAN was created to address the deficiencies in the current state of the art in long reach manipulators by utilizing an antagonistic tendon design [6]. TALISMAN simplified joint design and enhanced mechanical advantage by removing the motors from the joints themselves and reduced the size and power requirements for the overall control train. The system improved operational robustness, active antagonistic control, and reduced motor torque requirements [6]. The work also proved the case for cable-driven manipulation systems for in-space assembly and servicing operations.

B. COMPLIANT SPACE ROBOTICS

Compliant robotic systems provide unique capabilities and advantages regarding the space environment. Less rigid structures are more difficult to damage resulting in a more robust system. This is crucial for environments that are far from human contact and influence. A more durable and robust system allows for decision making with an incomplete information set. This decreases risk and increases the system's capability with respect to exploring unknown environments. Thus far, research in this area has focused on mobility for exploration, muscular assistance, and human space suit augmentation.

For surface exploration, Yale's TT-3 [7] and JPL's tumbleweed [8] ball have used the concept of tensegrity and inflatables respectively as novel methods of traversing difficult and unknown surface conditions. Omniskins [9] are adaptable skins that can be wrapped around various objects (e.g. Rocks) giving them the potential for mobility. For liquid environments such as Jupiter's Moon Europa, which is believed to host water oceans under its surface, Cornell has explored a squid like robot referred to as Roboeel [10].

Additionally, human space suits resist astronaut mobility, significantly increasing fatigue and limiting EVA duration. Augmenting human motion with soft actuators inside a suit is an active area of research. Shape memory alloy (NiTi – muscle wire) has been investigated as an additional tendon embedded in a suit to assist in joint mobility [11]. However, cable driven systems, more specifically, continuum systems, have the advantage of an infinite number of degrees of freedom (DOF) such that they can theoretically bend at any position along the length of the manipulator. This characteristic affords the manipulator the ability to work in confined spaces and in environments that can be both unknown and complex. This makes cable-driven continuum robotic manipulators of great interest for in-space assembly operations both on-orbit and on planetary surfaces where neither full human presence nor knowledge of the surface can be guaranteed.

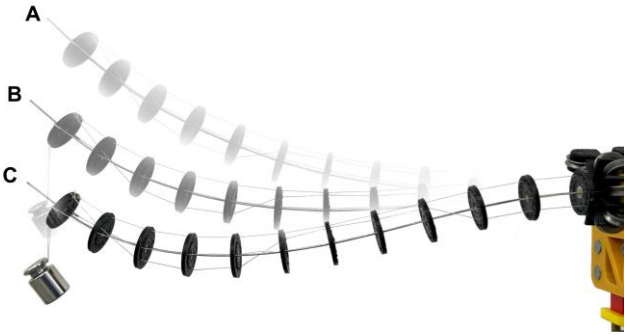

FIGURE 1. Behavior of a cable-driven continuum robot with a traditional straight tendon routing under a transverse gravity loading. The underactuated nature of the system is seen explicitly as load increases with a fixed cable displacement. A. Cable driven continuum robot under only self-weight in a cantilevered configuration. B. Robot under an additional 10g gravity loading at the end-effector. C. Robot under a 20 g gravity loading.

C. CONTRIBUTIONS

Fig. 1 shows a typical cable-driven continuum manipulator with an actuating cable located at a fixed radius to a slender elastic backbone and pulled to change the length of the cable and therefore the shape of the robot. A transverse gravity loading is applied at the end effector, and the deformation shown occurs because of the loading. Despite a fixed cable displacement, the stiffness at the end-effector remains relatively low since unactuated modes of deformation always exist which do not change the length of the tendon, yet which are associated with transverse displacement of the end-effector. The single cable provides a mechanical forcing which biases the robot shape towards an upward-facing curve, but additional cables would be required to increase the output stiffness, or stated equivalently, to gain control of additional modes of deformation in the flexible structure.

Cable- or tendon-driven robots with a cable path that varies substantially along the length of the robot are not well explored relative to designs with trivial or obvious cable paths such as a constant radius to the backbone of the robot. Mechanics-based models for general tendon routing are known [12], [13]. It is known that cable paths which cross over the backbone can be used to create "S" shapes in continuum robots and that various cable routing strategies can reduce coupling between independent joints in multi-joint continuum robots [14]. It is also known that both the cable path relative to the backbone and the stiffness of the cable against changes in length has a very large effect on the observable stiffness and loading behavior of the robot. Cable

paths which converge or diverge along the length of the robot produce large changes in the stiffness distribution, and the behavior under prescribed cable tension (low cable stiffness), vs. prescribed cable displacement (high cable stiffness), is fundamentally different [15].

In this work, we explore the design of cable-driven continuum robots with complex cable routings and with multiple, independent cables acting within the same region of the robot. We focus solely on planar designs in this initial work for the sake of clarity; the theory can be extended to spatially actuated robots. We extend previous modeling approaches to show for the first time that additional cables can be added which couple only weakly to a previous set of cables. Existing models of cable-driven continuum robots are extended to produce a theoretical design condition under which cable lengths are decoupled to the first order, providing independent control over multiple modes of deformation with minimal length coupling of the tendons. We demonstrate that the stiffness of the robot to external loads can be increased at least by a factor of 10, and that the distribution of stiffness along the robot's length can be substantially modified, by the introduction of a second set of cables which do not interfere with the operation of cables at a constant radius.

II. METHODS & MATERIALS

A. MODELING ASSUMPTIONS

Our modeling approach follows the Cosserat-rod based approach of Rucker et al. [12] and also incorporates the modal shape function approach of Chirikjian and Burdick [16]. The shape of the robot is assumed to be modeled by a single planar curve which is parameterized by arc length. The position of the neutral axis of the slender backbone, with respect to a fixed frame of reference, is denoted $\vec{p}: D \to E^3$ where $D = [0, L]$, and L is the length of the robot. The independent arc length variable is $s \in D$. The curve is framed by the addition of an arc-length parameterized frame of reference $\mathcal{F}(s)$ having origin $\vec{p}(s)$ and orthogonal director vectors $\vec{d}_1(s)$ tangent to the curve and $\vec{d}_2$ and $\vec{d}_3$ spanning the cross sections normal to the curve. The following modeling assumptions are adopted:

A1. The cross sections normal to the backbone curve remain planar and do not deform (Euler-Bernoulli bending hypothesis)

A2. The path of the i^{th} cable is described by a vector-valued function $\vec{r}_i(s)$, where the cable position is

$$\vec{p}_i(s) = \vec{p}(s) + \vec{r}_i(s) \tag{1}$$

and the vector $\vec{r}_i$ is stationary with respect to changes in the configuration when measured in the frame of reference $\mathcal{F}(s)$. In other words,

$$\vec{r}_i(s) = r_{i2}(s)\vec{d}_2(s) \tag{2}$$

A3. The cables are perfectly inextensible

A4. The function r_{i2} is differentiable with respect to s

A5. The internal moment is linearly related to the local curvature $\kappa(s)$ as

$$m(s) = k_b(s)\kappa(s) \tag{3}$$

A6. The robot shape is planar, and the backbone position and director vectors satisfy the following kinematic hypotheses implying that shear and extension are negligible

$$\frac{d\vec{d}_k}{ds} = \vec{\kappa} \times \vec{d}_k \tag{4}$$

$$\frac{d\vec{p}}{ds} = \vec{d}_1 \tag{5}$$

$$\vec{\kappa}(s) = \kappa(s)\vec{d}_3(s) \tag{6}$$

A7. The curvature $\kappa(s)$ is assumed to be differentiable.

A8. The reference, stress-free configuration of the backbone is straight.

B. PRELIMINARIES

Definition 1: The energy inner product is the bilinear form $\langle \cdot, \cdot \rangle : V \times V \to \mathbb{R}$ defined by

$$\langle a, b \rangle_{k_b} = \frac{1}{2}\int_0^L k_b(\sigma)a(\sigma)b(\sigma)\, d\sigma \tag{7}$$

Definition 2: The energy norm is given by

$$\|\kappa\|_{k_b} = \langle \kappa, \kappa \rangle \tag{8}$$

Definition 3: An orthonormal basis B is given such that

$$B = \{\phi_k \mid k = 1, \dots, \infty\}, \tag{9}$$

and

$$\langle \phi_i, \phi_k \rangle_{k_b} = \delta_{ik}\,, \tag{10}$$

where δ_{ik} is the Kronecker delta.

Then, we may write the curvature as a sum of weighted curvature modes.

$$\kappa(s) = \sum_{i=1}^{\infty} q_i \phi_i(s) \tag{11}$$

Definition 4: Each of the normalized basis functions ϕ_i is called a *curvature mode*.

A finite approximation to the sum suffices for engineering purposes. Therefore, the configuration space $\mathcal{C} = \mathbb{R}^m$ and $q = (q_1, \dots, q_m) \in \mathcal{C}$. Because each basis function ϕ is normalized with respect to the energy norm, it has dimension of $F^{-0.5}L^{-1.5}$ (F = Force, L = Length). The generalized coordinates have dimension $F^{0.5}L^{0.5}$, which is the square root of the dimension of energy. The kinematic differential equations imply that a solution $p(s)$ is given when q is known and when initial conditions $\vec{p}_0$ and $\vec{d}_{k0}$ are known.

Lemma 1: The length of the i^{th} cable is calculated by the cable length functional

$$L_i(q) = L_i[\kappa(q)] = \int_0^L g_i\big(\kappa(\sigma)\big)\, d\sigma \tag{12}$$

$$g_i(\kappa) = \sqrt{(r_{i2}')^2 + (1 - r_{i2}\kappa)^2} \tag{13}$$

Proof: The length of the cable is given by

$$L_i(q) = \int_0^L \left\| \frac{d\vec{p}_i}{ds} \right\| ds \tag{14}$$

Calculating,

$$\left\| \frac{d\vec{p}_i}{ds} \right\| = \left\| \vec{d}_1 + \vec{\kappa} \times \vec{r}_i + \frac{dr_{i2}}{ds}\vec{d}_2(s) \right\| = g_i(\kappa) \tag{15}$$

□

C. PERFECT CABLE DECOUPLING

We define the notion of perfectly decoupled cables to mean that n cable paths admit a choice of curvature modes so that the configuration space Q may be partitioned into a direct sum

$$Q = Q_1 \oplus Q_2 \oplus \cdots \oplus Q_n \oplus Q_{n+1} \tag{16}$$

such that each cable length depends only on one of the vector subspaces:

$$\begin{aligned} L_1(q) &= L_1(q_1), \qquad q_1 \in Q_1 \\ L_2(q) &= L_2(q_2), \qquad q_2 \in Q_2 \\ &\vdots \\ L_n(q) &= L_n(q_n), \qquad q_n \in Q_n \end{aligned} \tag{17}$$

The subspace Q_{n+1} consists of the coordinates along curvature modes which do not affect the length of any cable.

Thus, any configuration q may be written as a sum of components

$$q = q_1 + q_2 + \cdots + q_n + q_{n+1} \tag{18}$$

Due to the series (8) and the orthonormality of the basis B, the subspaces Q_i are in direct one-to-one correspondence with subspaces V_i such that

$$\kappa = \kappa_1 + \cdots + \kappa_n + \kappa_{n+1} \tag{19}$$

These conditions state that the robot deformations can be partitioned into a sum of component deformations in which each component is associated with only a single cable or subset of cables. A natural question is "what cable path designs $r_{i2}(s)$ admit such perfect cable decoupling?"

One obvious solution to the mathematical question emerges, which is simply to locate the cable at zero radius to the backbone over all regions of the length except over a finite number of support regions. For example, divide the domain $D = [0, L]$ into two subdomains $D_1 = [0, a]$ and $D_2 = [a, L]$. If the cable shape function $r_{12}(s)$ has support only on D_1 and $r_{22}(s)$ only on D_2, then the cables are perfectly decoupled. The corresponding spaces Q_1 and Q_2 are associated with curvature modes having support over the same subdomains, much like a serial kinematic structure. Practically speaking, any implementation of this strategy would require some means of routing a cable with zero radius to the backbone over some finite subset of the robot length or would require the placement of actuators at multiple places along the robot. Note that it is not enough to route cables from the base of a robot and have some cables terminate early before reaching the end. Doing so results in coupled cables, which motivated work on solving the coupled inverse kinematics problem [17].

D. APPROXIMATE CABLE DECOUPLING

Cables can be approximately decoupled by forcing the cable length functions to have gradients satisfying a condition of independence at a single point $q \in Q$.

$$\nabla_q L_i \cdot e_j = 0, \qquad \forall\, i \neq j \tag{20}$$

Define the first partial derivative

$$\frac{\partial L_i}{\partial q_j} \triangleq \int_0^L F_{ij}\big(r_i, r_i', \kappa, \phi_j\big)\, ds \tag{21}$$

Theorem 2: The cables lengths are locally decoupled at $q = 0$ if the following design condition applies to the cable routes.

$$\frac{r_i}{\sqrt{1 + (r_i')^2}} = \alpha k_b \phi_i \tag{22}$$

The parameter $\alpha \in \mathbb{R}\backslash 0$ is a free choice.

Proof: Consider the Taylor expansion of F_{ij} about the point $\kappa = 0$.

$$F_{ij} = \frac{r_{i2}\phi_j}{g_i(0)} + \mathcal{O}(\kappa) \tag{23}$$

Defining F_{ij0} to be the zeroth order (constant) term of the expansion, the independence of cable length i on mode j requires

$$\int_0^L \frac{r_{i2}}{g_i(0)}\phi_j\, ds = 0 \tag{24}$$

By choice of r_{i2}, let

$$\frac{r_{i2}}{g_i(0)} = \alpha k_b \phi_i \tag{25}$$

Then, for all $i \neq j$

$$\left.\frac{\partial L_i}{\partial q_j}\right|_{q=0} = \alpha\langle \phi_i, \phi_j \rangle_{k_b} = 0 \tag{26}$$

□

The scale parameter α has dimension $\mathrm{F}^{-0.5}\mathrm{L}^{0.5}$ to ensure dimensional homogeneity of (16). As one example of a pair of orthogonal modes, consider the following choices

$$\phi_1 = \frac{1}{\sqrt{Lk_b}}$$
$$\phi_2 = \frac{\sqrt{2}}{\sqrt{Lk_b}} cos\left(\frac{\pi s}{L}\right) \quad (27)$$

which satisfy the orthogonality condition for any robot having uniform (constant in arc length) flexural rigidity k_b. The first curvature mode corresponds to circular bending (i.e., "constant curvature"), and the cable shape r_{12} is the usual straight cables at a constant radius to the backbone. The cable shapes r_{i2}, in a geometric sense independent of scale, are determined by the dimensionless group

$$\Pi_1 = \frac{\alpha\sqrt{k_b}}{L^{1.5}} \quad (28)$$

For small values of Π_1, the cable shapes mimic the right-hand side of (19), i.e. $r_{i2} \approx \alpha k_b \phi_i$. As Π_1 increases, the cable shape begins to change substantially (**Error! Reference source not found.**). The solutions found to (22) for ϕ_2 as in (27) demonstrate a critical value of α at which the cable path folds back on itself, implying that the robot must be sufficiently slender for this design approach to be practical since "folded" cable paths may be difficult to support mechanically and may also cause high cable friction.

The critical value of Π_1 depends on the specific functional basis chosen. For example, if instead ϕ_2 is a linear function,

$$\phi_2 = \frac{\sqrt{3}}{\sqrt{Lk_b}}\left(1 - \frac{2s}{L}\right) \quad (29)$$

then the solution r_{22} can be found by ansatz as $r_{22} = mx + b$, where the parameters are given by

$$m = -\frac{2\sqrt{3}\Pi_1}{\sqrt{1 - 12\Pi_1^2}} \quad (30)$$

$$b = \frac{\sqrt{3}\Pi_1 L}{\sqrt{1 - 12\Pi_1^2}} \quad (31)$$

The critical value for linear cable paths is therefore

$$\Pi_1^* = \sqrt{1/12} \approx 0.2887 \quad (32)$$

The decoupled cable design also results in a simple relationship between the tension in the cables and the resulting robot shapes if the deflections remain small. With orthonormal curvature modes and cable routes designed according to the conditions of Theorem 2, the generalized coordinates and the cable tension increments t_i (above the pretension) are approximately related by

$$t_i \approx \frac{2q_i}{\alpha_i} \quad (33)$$

To prove this, consider static equilibrium on a section. The total internal moment in the backbone must be equal to m, calculated as follows.

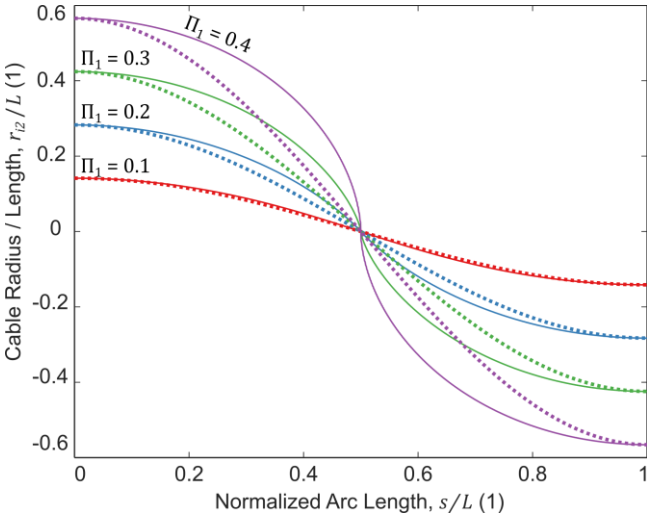

FIGURE 2. Cable shapes for ϕ_2 described by (27). Solid lines depict the cable paths solving the design condition of Theorem 2. Dashed lines correspond to the right side of (22). The shape and scale of the cable path, normalized by the length of the backbone, is determined by the dimensionless parameter Π_1. At a critical value near $\Pi_1 = 0.4$, the cable path crosses the backbone of the robot nearly perpendicularly.

$$m = \sum_{i=1}^{n} t_i r_i \, cos\, \gamma_i \quad (34)$$

The angle γ_i is the angle between the tangent to the cable path cable and the tangent to the backbone. For small curvatures it may be approximated as

$$cos\, \gamma_i \approx \frac{1}{\sqrt{1 + (r_i')^2}} \quad (35)$$

Based on the assumption (3), the elastic energy is

$$E = \frac{1}{2}\int_0^L m\kappa \, ds = \frac{1}{2}\sum_{i=1}^{\infty} q_i^2 \quad (36)$$

By application of the cable design condition, calculation of the moment in terms of the cable tensions, and direct substitution,

$$E \approx \frac{1}{2}\int_0^L \left(\sum_{i=1}^{n} \frac{t_i r_i(s)}{\sqrt{1 + r_i'(s)^2}}\right)\left(\sum_{i=1}^{\infty} q_i \phi_i(s)\right) ds = \frac{1}{2}\sum_{i=1}^{n} c_i t_i q_i \quad (37)$$

where

$$c_i = \alpha_i \langle \phi_i, \phi_i \rangle_{k_b} = \alpha_i \quad (38)$$

Then the cable tension is calculated as

$$t_i \approx \frac{2}{c_i}\frac{\partial E}{\partial q_i} \quad (39)$$

The result (33) follows by direct calculation.

This result demonstrates that the interpretation of the scale parameter α_i is approximately the inverse of half the cable

tension required to create a unit of deformation along the coordinate q_i. A unit deformation along q_i stores one unit of elastic energy by virtue of its definition, with the unit of measure determined by the units of ϕ_i and k_b.

The orthogonality of the curvature basis also provides a convenient calculation of the component of the cable tensions due to the elastic forces for an arbitrary configuration of the robot, which follows directly from Theorem 3 and the definition of the energy inner product:

$$t_i \approx \frac{2}{\alpha_i}\langle \kappa, \phi_i \rangle_{k_b} \tag{40}$$

If the cables are pretensioned, then this calculated tension due to the elastic internal forces is simply superposed on the pretension to arrive at the final cable tension. Note that this approximate calculation should not be understood as a method of calculating the tensions that will produce a given shape, since in general an arbitrary specification of the shape would require an infinite number of cables to achieve.

E. CABLE STIFFENING

The preceding analysis also implies that in a traditionally designed cable-driven continuum robot having only a single pair of cables that antagonistically actuate a constant-curvature mode, the actuating cable has little effect on the apparent stiffness of higher-order curvature modes. Curvature along these higher-order modes does not substantially change the length of the actuating cable, at least in the sense of small deflections, and the tension in the cable is approximately independent of these other modes.

The approximate cable decoupling condition suggests a means of modifying the natural compliance of cable-driven robots through the addition of cables that are routed so that the cable lengths couple weakly to the actuated curvature modes of the robot. We designed a robot having an actuated constant curvature mode and a stiffened sinusoidal curvature mode using an additional pair of cables routed in the appropriate shape $r_{i2}(s)$ which was generated by ϕ_2 as in (27). These additional cables are pretensioned and locked off. In other words, the additional stiffening cables are unactuated, and the length of cable is constant. The constant curvature actuating cables are a single cable loop driven by a manually controlled, self-locking worm wheel which drives a short segment of a timing belt to which the cables are attached. The cables are made from commercially available braided ultra-high molecular weight polyethylene fishing line with a strength of 10 lb test. The backbone of the robot is made from a 2-ply carbon fiber (CF)/epoxy laminate, manufactured by resin infusion, with a final thickness of 0.59 mm (Composite Envisions, Wausau, WI, USA). The CF is a 3K plain weave fabric and was stacked in a symmetric layup with respect to the laminate's geometric mid-plane. The prototype has the dimensions shown in Table I. The prototype design and a photograph are shown in Figure 3. The cable support radii are described in Table II.

TABLE I
PROTOTYPE ROBOT DESIGN PARAMETERS.

Parameter	Symbol	Value
Backbone length	L	270 mm
Backbone height	h	60 mm
No. of cable supports	N	7
Cable support spacing	ΔL	45 mm
Backbone thickness	t	0.59 mm

TABLE II
PROTOTYPE CABLE SUPPORT LOCATIONS AND RADII

Support Index, i	Support location, s_i (mm)	r_{12} (mm)	r_{22} (mm)
1	0	30.0	25.0
2	45	30.0	21.7
3	90	30.0	12.5
4	135	30.0	0
5	180	30.0	−12.5
6	225	30.0	−21.7
7	270	30.0	−25.0

F. KINEMATIC SIMULATION

To verify that the approximate decoupling at zero curvature is a practical design condition, we simulated the kinematics of a cable-driven robot using the constant and cosine curvature modes. The robot is assumed to be actuated using the constant radius cables, which apply a forcing that tends to actuate the constant curvature mode. The backbone curve is simulated according to the piecewise constant curvature method described by Webster and Jones [18]. The cable lengths for each of the four cables (two antagonistic pairs) is modeled by the sum of the distances between the cable support holes.

G. STIFFNESS MEASUREMENT

To assess the influence of the stiffening cables on the mechanical performance of the robot, we used an industrial robot manipulator (UR5e, Universal Robots) to produce controlled displacements of the robot backbone while measuring the reaction force with a load cell (LCMFL-20N, OMEGA, Norwalk, CT, USA). The experimental setup is depicted in Figure 6. Analog voltage samples were taken at 30 Hz. The base of the cable-driven continuum robot was fixed to a support structure mounted to the same table as the UR5e robot base. The UR5e was programmed to displace the continuum robot by contacting it at each of the cable support structures in sequence. The maximum displacement of each support disc was approximately 5 mm. The same controlled displacement profile was used for all trials. The motion of the UR5e end-effector was tracked by a three-camera OptiTrack motion capture system set to acquire frames at 30 Hz. After data acquisition, a manual coordinate system rotation was performed to align the displacement during contacts to the x-axis of the coordinate system. The peaks in the x-displacement and the force timeseries were identified manually and a region around each peak of length 300

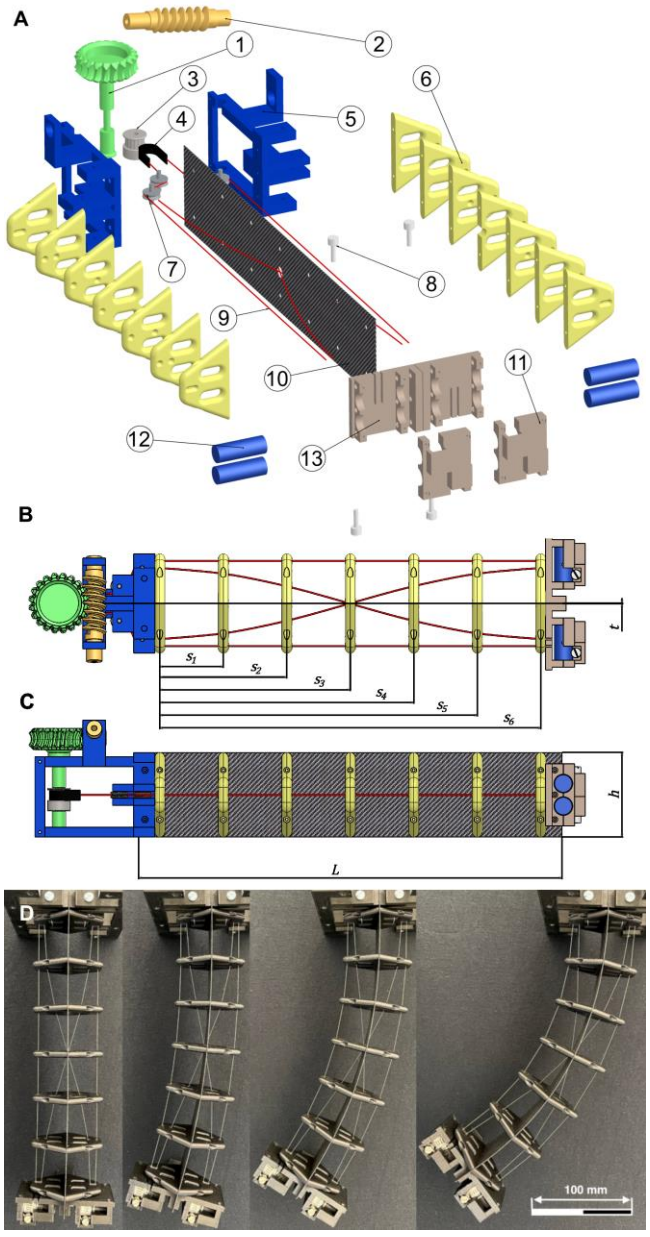

FIGURE 3. **A. Exploded view. ① Worm gear ② worm ③ timing pulley ④timing belt segment ⑤ base frame ⑥ cable supports ⑦ cable routing pulleys ⑧ fasteners ⑨ cables ⑩ carbon fiber backbone ⑪ tensioner clamp ⑫ tensioner barrel ⑬ tensioner housing B. Top view (assembled). C. Side view (assembled). D. Sequence (left-to-right) of increasing curvature caused by turning the worm. All cables are pretensioned. See Tables I and II for values of dimensions.**

samples was segmented to produce a force vs. displacement response for contact forces at the cable support structure

The entire experiment was repeated three times, and a linear model of the following form was fit to the data by least squares regression.

$$F_{kl} = \beta_k x + \eta_{kl} \tag{41}$$

The index $k = 1, \ldots, 7$ indicates the contact location and the index $l = 1,2,3$ indicates the experimental repetition. β_k are the stiffnesses observed at each contact location (i.e. both the force and displacement are measured at the contact location),

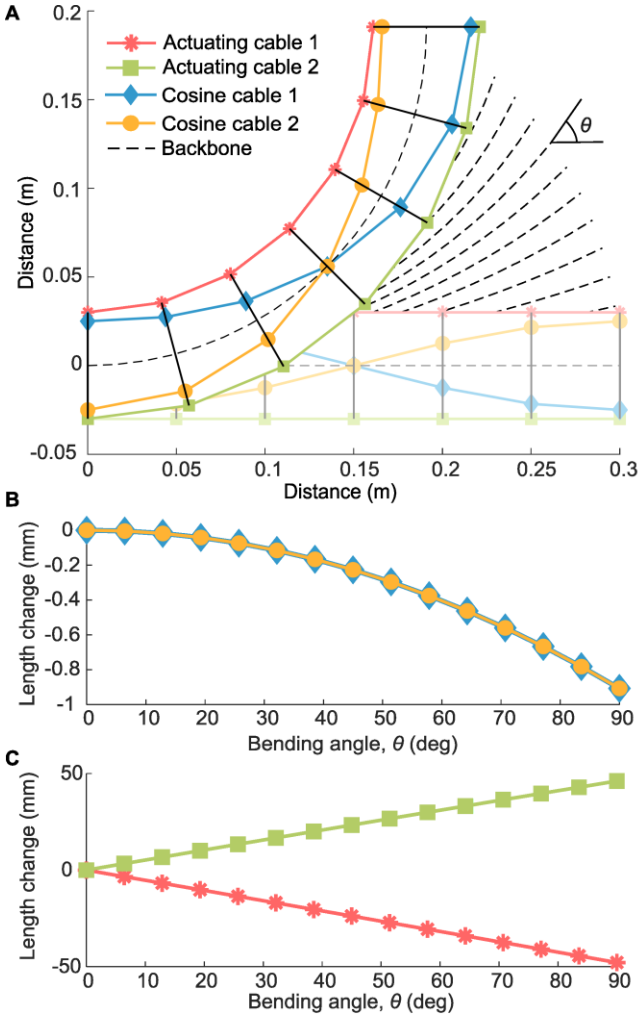

FIGURE 4. **A. Simulation of constant-curvature bending of the backbone. Cable supports are treated as rigid bodies, and cable lengths are calculated by the sum of point-to-point Euclidean distance between the supports. B. Length change of the stiffening cable paths as the robot bends. C. Length change of the actuating cable paths as the robot bends.**

x is the rotated end-effector coordinate of the UR5, and η_{kl} is a contact-location and repetition-dependent bias term.

III. RESULTS

A. KINEMATIC SIMULATION

For the prototype design parameters, the total path length for the stiffening cables changes only by 0.88 mm over a change in robot bending angle from 0° to 90°. The sum of the actuating cable lengths changes by a similar amount.

B. STIFFNESS MEASUREMENT

Time series data from one trial of the experiment with all cables pretensioned is shown in Fig. 4. The segmentations of each trial were used to construct the linear regression model described by (30). The stiffness parameters β_k are shown for each pre-tensioning case and at each location of applied force in Fig. 5. Statistically significant differences in the stiffness of the robot are evident depending on which cables are pretensioned and which are slacked. The stiffness is greatest

FIGURE 5. **Experimental setup for stiffness characterization of the cable-driven continuum robot for contact forces applied at different locations along the robot.**

at each location when all cables are pretensioned, indicating that, at least for the design and range of pre-tensions tested, it is not possible for an increase in pre-tension to result in a decrease in observable stiffness.

The results shown in Fig. 7 demonstrate that the end-effector stiffness, which is measured at the furthest point from the fixed base, is similar between cases N (no cables) and C (stiffening cables only). This is expected because a force applied at the end-effector will tend to produce deformation along the lowest order mode more than the higher modes. In the case of no cables, the deflection is approximately a third order polynomial with distance (the classic Euler-Bernoulli beam solution for cantilevered loads applied on uniform beams). The cosine-shaped cables are designed to match a mode which is orthogonal to the lowest

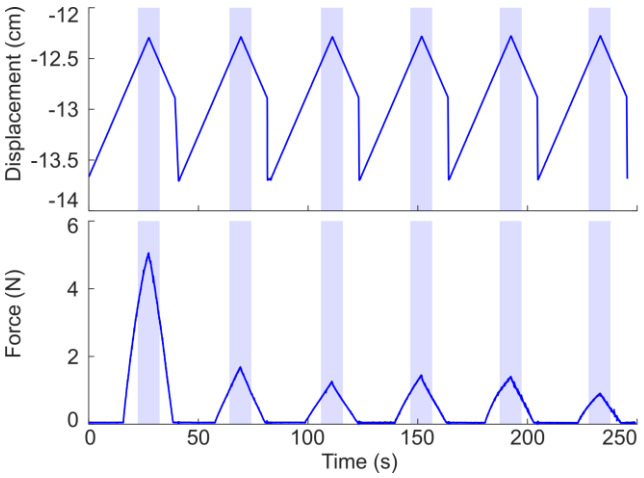

FIGURE 6. **Force and displacement data captured during trial 1 of the case with all cables pretensioned. The manual segmentation of the data is overlaid as blue shading. Contact between the UR5 and the robot under test exists whenever the force is nonzero.**

order constant-curvature mode. On the other hand, when all cables are pretensioned, the response of the structure is substantially different than in any of the other conditions. Most notably, the end-effector stiffness is increased by approximately a factor of 14 when compared to case N and a factor of 10 when compared to case A, which is the most common case found in prior literature. However, at the midpoint of the robot, the stiffness increase is only a factor of 3.45 times higher than case N and 5 times higher than case A.

IV. DISCUSSION

When the cables are designed according to Theorem 2, the cable lengths are approximately decoupled, and each cable's tension couples predominantly to the mode for which it is designed, as illustrated clearly by (33). The implication of this is that even though *perfect* decoupling is not possible, small amounts of stretch allowed in the cables and cable support structures means that all cables, even those which are tied off and have an ostensibly fixed length, may remain taut even when the robot undergoes large deflections.

The stiffness of the cable-driven robot is modified substantially by the introduction of the additional stiffening cables which are designed according to the conditions of Theorem 2. In particular, the distribution of stiffness is altered fundamentally from the typical inverse cube law for the stiffness of a cantilevered structure. An interesting observation is that when all cables are pretensioned, the stiffness at the fourth cable support is higher than the stiffness at the third support, which is atypical for a cantilevered structure. It is noteworthy that this is the location where the stiffening cable crosses over the backbone. This result is expected, and one way to explain it is that the next higher mode in the orthogonal trigonometric series is $\cos(2\pi s/L)$, over which the stiffening cable has little influence. For small deflections, this next mode is associated with deflections that are the second integral of the

curvature, which has a maximum exactly at the point where the stiffness is measured to be a minimum.

Since the orthogonality condition in Definition 3 is general, one avenue for future work is to understand how the choice of basis affects the properties of the resulting robot. The orthogonal trigonometric sequence is not the only orthogonal function sequence which can form a curvature basis. For example, the cosine and linear cable shapes are two of infinitely many alternatives for cable designs that are orthogonal to a straight cable. Future work is needed to determine the advantages and disadvantages to specific selections of the basis.

Although not quantified experimentally, we observed through direct manipulation of the robot by hand that in the experimental condition with all cables pretensioned, the stiffness of the end-effector to applied torques in the plane of bending was vastly increased in comparison to the case in which only the actuating cables are pretensioned.

One limitation of the overall strategy is that the additional cables increase the compressive preload in the backbone member. At some critical load, the backbone itself may buckle between the cable tie off points. On the other hand, the buckling modes are themselves deformations of the backbone which may be controlled by the additional cables. The balance of these effects should also be investigated in future work.

V. CONCLUSION

Cable driven continuum manipulators provide in-space assembly with interesting solutions to the problems envisioned in building and maintaining large space structures and surface support infrastructure, requiring flexibility and adaptability in unstructured and uncertain environments. However, these systems, given their possibly infinite-dimensional deformation characteristics provide a continuing challenge in modeling and control. This work provides a strategy and next steps in addressing this problem towards a methodology to address uncontrolled deformation. This work will enable future designs for both terrestrial and extraterrestrial uses.

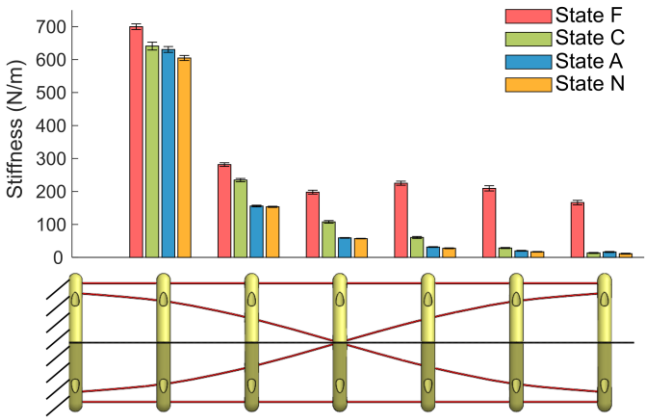

FIGURE 7. Stiffness along the length of the cable-driven robot with one fixed boundary condition. Bars indicate stiffness and are grouped by physical location of the measurement (at each of the cable support structures). Whiskers indicate the 95% confidence intervals of the parameter estimates. Stiffness is measured across the factor of condition of cable pretensioning with the factors being (N) no cables pretensioned, (A) actuating cables only pretensioned, (C) stiffening cables only pretensioned, (F) all cables pretensioned. Whiskers on the bars indicate the 95% confidence interval of the linear model coefficients.

REFERENCES

[1] W. Doggett, "Robotic assembly of truss structures for space systems and future research plans," in *Proceedings, IEEE Aerospace Conference*, Mar. 2002, vol. 7, pp. 7–7. doi: 10.1109/AERO.2002.1035335.

[2] J. Lymer, "NASA's Dragonfly Program: Commercialized Robotics - Enabling a New Generation of Evolvable, Resilient Assets in Orbit," presented at the 35th Space Symposium, Technical Track, 2018.

[3] S. Patane, E. R. Joyce, M. P. Snyder, and P. Shestople, "Archinaut: In-Space Manufacturing and Assembly for Next-Generation Space Habitats," in *AIAA SPACE and Astronautics Forum and Exposition*, American Institute of Aeronautics and Astronautics. doi: 10.2514/6.2017-5227.

[4] L. M. Bowman, W. K. Belvin, E. E. Komendera, J. T. Dorsey, and B. R. Doggett, "In-space assembly application and technology for NASA's future science observatory and platform missions," in *Space Telescopes and Instrumentation 2018: Optical, Infrared, and Millimeter Wave*, Jul. 2018, vol. 10698, pp. 690–708. doi: 10.1117/12.2311413.

[5] R. Mukherjee *et al.*, "When is it Worth Assembling Observatories in Space?," in *Bulletin of the American Astronomical Society, Astro2020: Decadal Survey on Astronomy and Astrophysics*, 2019, vol. 51, p. 50.

[6] M. Mahlin, R. L. Wagner, J. Dorsey, and T. C. Jones, "Tendon-Actuated Lightweight In-Space MANipulator (TALISMAN) Hinge Joint Structural," in *ASCEND 2020*, American Institute of Aeronautics and Astronautics. doi: 10.2514/6.2020-4251.

[7] L.-H. Chen *et al.*, "Soft Spherical Tensegrity Robot Design Using Rod-Centered Actuation and Control," *J. Mech. Robot.*, vol. 9, no. 2, Mar. 2017, doi: 10.1115/1.4036014.

[8] J. A. Jones, "Inflatable Robotics for Planetary Applications," in *International Symposium on Artificial Intelligence, Robotics and Automation in Space (i-SAIRAS)*, Quebec, Canada, 2001, pp. 1–6.

[9] J. W. Booth *et al.*, "OmniSkins: Robotic skins that turn inanimate objects into multifunctional robots," *Sci. Robot.*, vol. 3, no. 22, p. eaat1853, Sep. 2018, doi: 10.1126/scirobotics.aat1853.

[10] M. Peck, "Soft-Robotic Rover with Electrodynamic Power Scavenging," Cornell, Ithaca, NY, NIAC Phase 1 Final Report, Mar. 2016. Accessed: May 20, 2022. [Online]. Available: https://www.nasa.gov/sites/default/files/atoms/files/11-2015_phase_i_mason_peck_soft_robotic_rover_electrodynamic_power_scavenging.pdf

[11] B. T. Holschuh and D. J. Newman, "Morphing Compression Garments for Space Medicine and Extravehicular Activity Using Active Materials," *Aerosp. Med. Hum. Perform.*, vol. 87, no. 2, pp. 84–92, Feb. 2016, doi: 10.3357/AMHP.4349.2016.

[12] D. C. Rucker and R. J. Webster III, "Statics and Dynamics of Continuum Robots With General Tendon Routing and External Loading," *IEEE Trans. Robot.*, vol. 27, no. 6, pp. 1033–1044, Dec. 2011, doi: 10.1109/TRO.2011.2160469.

[13] P. Rao, Q. Peyron, S. Lilge, and J. Burgner-Kahrs, "How to Model Tendon-Driven Continuum Robots and Benchmark Modelling Performance," *Front. Robot. AI*, vol. 7, p. 630245, Feb. 2021, doi: 10.3389/frobt.2020.630245.

[14] Y. Chitalia, S. Jeong, N. Deaton, J. J. Chern, and J. P. Desai, "Design and Kinematics Analysis of a Robotic Pediatric Neuroendoscope Tool Body," *IEEEASME Trans. Mechatron.*, vol. 25, no. 2, pp. 985–995, Apr. 2020, doi: 10.1109/TMECH.2020.2967748.

[15] K. Oliver-Butler, J. Till, and C. Rucker, "Continuum Robot Stiffness Under External Loads and Prescribed Tendon Displacements," *IEEE Trans. Robot.*, vol. 35, no. 2, pp. 403–419, Apr. 2019, doi: 10.1109/TRO.2018.2885923.

[16] G. S. Chirikjian and J. W. Burdick, "A modal approach to hyper-redundant manipulator kinematics," *IEEE Trans. Robot. Autom.*, vol. 10, no. 3, pp. 343–354, Jun. 1994, doi: 10.1109/70.294209.
[17] B. A. Jones and I. D. Walker, "Practical Kinematics for Real-Time Implementation of Continuum Robots," *IEEE Trans. Robot.*, vol. 22, no. 6, pp. 1087–1099, Dec. 2006, doi: 10.1109/TRO.2006.886268.